Research Square

Preprints are preliminary reports that have not undergone peer review.
They should not be considered conclusive, used to inform clinical practice,
or referenced by the media as validated information.

Biomechanical Adaptations and Dynamic Stability Control During Firefighter Rescue Running Under Fatigue and Shoulder-Carried Load Conditions

Min Chen

[illegible]

Jie Wang

Hohai University

Guangliang Fu

Tianjin University of Sport

Weiguo Liu

liuwg@mailbox.gxnu.edu.cn

[illegible]

Article

Keywords: firefighter, occupational biomechanics, fatigue, shoulder-carried load

Posted Date: November 23rd, 2026

DOI: https://doi.org/10.21203/rs.3.rs-11509637/v1

License: This work is licensed under a Creative Commons Attribution 4.0 International License.
Read Full License

Additional Declarations: No competing interests reported.

Biomechanical Adaptations and Dynamic Stability Control During Firefighter Rescue Running Under Fatigue and Shoulder-Carried Load Conditions

Min Chen[1,2],Jie Wang[3],Guangliang Fu[4*] †, Weiguo Liu[1*] †

1 College of Physical Education and Health, Guangxi Normal University,541006, Guilin, China

2 School of Physical Education and Art，East China University of Technology,344199,Fuzhou,China

3 Department of Physical Education, Hohai University,210024, Nanjing,China

4 School of Sports Training, Tianjin University of Sport,300211,Tianjin,China

Corresponding author(s). E-mail(s): 202320300025@stu.tjus.edu.cn; liuwg@mailbox.gxnu.edu.cn;

Introduction: Firefighters frequently perform emergency rescue running while experiencing fatigue and carrying task-specific loads, which may challenge movement control and increase the risk of musculoskeletal injury. However, the combined effects of fatigue and shoulder-carried load on occupational movement adaptation and dynamic stability remain insufficiently understood. This study aimed to investigate how fatigue and shoulder-carried load influence lower-limb biomechanics and dynamic stability during firefighter rescue running.

Methods: Seventeen male firefighters completed rescue-running trials under two fatigue states (pre-fatigue and post-fatigue) and three shoulder-carried load conditions (10, 20, and 30 kg) using a repeated-measures experimental design. Three-dimensional kinematics and ground reaction forces were collected during the stance phase. Spatiotemporal parameters, lower-limb joint motion, joint moments, ground reaction forces, and center-of-gravity displacement were analyzed using linear mixed-effects models and one-dimensional statistical parametric mapping.

Results: Increasing load was associated with shorter steps (1.547, 1.441, and 1.341 m at 10, 20, and 30 kg, respectively; $P < 0.001$), load-related changes in positive peak hip and knee moments (both $P \leq 0.003$), lower peak vertical ground reaction force ($P < 0.001$), and reduced vertical COG excursion ($P < 0.001$). After fatigue, step width was lower (0.110 versus 0.080 m; $P = 0.018$), hip, knee, and ankle range of motion increased (all adjusted $q \leq 0.005$), and anteroposterior COG excursion increased ($P < 0.001$). Peak vertical ground reaction force also showed a fatigue main effect ($P = 0.001$). Mediolateral COG excursion showed no significant fixed effects. Waveform analysis identified load-related differences across portions of stance in joint angles, joint moments, ground reaction forces, and COG trajectories, complementing the discrete findings. Fatigue × load interactions were generally absent in the discrete outcomes.

Conclusions: Shoulder-carried load and fatigue were associated with different patterns of biomechanical change during firefighter rescue running. The combination of discrete and waveform analyses shows both which measures changed and when during stance the waveform differences occurred, offering a more detailed basis for evaluating loaded rescue tasks. However, COG displacement does not directly quantify dynamic stability. Because running speed was not verified for each condition and testing order was fixed, the observed changes cannot be attributed exclusively to load or fatigue, nor can their implications for balance or injury risk be established.

Keywords: firefighter; occupational biomechanics; fatigue; shoulder-carried load;

Introduction

Firefighters are frequently required to perform short-distance rescue running while wearing protective equipment and carrying task-specific tools or victims under urgent and hazardous conditions. These occupational demands expose firefighters to a high risk of work-related physical injury, particularly musculoskeletal disorders affecting the lower back and lower extremities [1,2]. In addition to the mass and movement restriction imposed by protective clothing, rescue operations often require asymmetric or shoulder-carried loads, such as fire hoses, compressed gas cylinders, and ladders. Such loads may alter gait regulation, postural control, and lower-limb mechanics, thereby increasing the physical burden of rescue running and potentially elevating the risk of slips, trips, falls, and overuse injury [3-5].

Firefighter rescue running is not simply a loaded form of ordinary running. Unlike backpack or vest loading, shoulder-carried loads are commonly positioned away from the body's midline and may create asymmetric moments around the trunk and pelvis. Previous firefighter studies have shown that simulated firefighting activities and asymmetric hose-load carriage shorten step and stride length and increase double-support time, suggesting that firefighters adopt a more cautious gait strategy when exposed to fatigue or asymmetric load [3]. Firefighting protective equipment has also been shown to restrict foot function, reduce center-of-pressure excursion, and increase foot-ground contact time, indicating impaired gait stability [4]. More recent work on firefighter rescue running further demonstrated that task-specific loads can reduce gait velocity and stride length, prolong support time, and increase hip and knee mechanical demand [5]. These findings indicate that loaded firefighter running involves coordinated changes across gait, joint mechanics, and stability control.

Fatigue is another critical constraint in rescue running because firefighters often perform high-intensity tasks after repeated exertion, heat exposure, stair climbing, hose handling, or victim rescue. Running-induced fatigue can modify spatiotemporal parameters, shock attenuation, joint kinematics, joint kinetics, and neuromuscular coordination [6-8]. Systematic reviews suggest that fatigue commonly increases ground contact time, reduces step length, alters lower-limb stiffness, and may redistribute mechanical demand from distal to proximal joints [6-8]. Although some joint-level variables may remain unchanged at the group level, fatigue can still affect movement control through changes in coordination variability and center-of-mass regulation [9,10]. Therefore, fatigue should be considered not only as a performance-limiting factor, but also as a neuromuscular control challenge that may alter how firefighters stabilize the body and distribute mechanical load during stance.

External load magnitude may further amplify or reshape these fatigue-related adaptations. Running with load has been shown to increase leg stiffness, ground contact time, and lower-limb joint flexion, suggesting that runners adopt a more crouched and mechanically stiff strategy to accommodate added mass [11]. Military load-carriage studies also report that load and fatigue can increase ground reaction forces and loading rates, supporting a potential link between loaded locomotion and lower-extremity overuse injury [12]. However, the direction of ground reaction force changes may depend on task context, speed regulation, and load-carrying strategy. For example, firefighter rescue tasks may reduce vertical ground reaction force when participants slow down or adopt a conservative gait strategy, even though internal joint demand may remain elevated [5]. Because ground reaction force does not always directly represent internal tissue loading, it should be interpreted together with joint moments, joint motion, and dynamic stability variables [13].

Dynamic stability provides an essential link between movement control and operational safety. Stability during locomotion depends on the control of the body's center of mass relative to the base of support, and different stability measures capture different aspects of this control [14]. The mediolateral direction is particularly important because lateral balance requires active regulation through foot placement, hip abductor activity, and trunk-pelvis control [15]. In rescue running, shoulder-carried load may shift the combined body-load center of mass and increase frontal-plane control demands, while fatigue may reduce the neuromuscular capacity to respond rapidly to perturbations. Thus, changes in center-of-gravity motion may reveal stability challenges that are not fully captured by discrete gait parameters or peak force measures.

Despite growing interest in firefighter biomechanics, several gaps remain. First, many studies have examined protective clothing, load carriage, or fatigue separately, whereas real rescue tasks expose firefighters to fatigue and external load simultaneously. Second, previous firefighter studies have often focused on walking, non-fatigued running, or isolated rescue tasks, leaving the combined effects of fatigue state and shoulder-carried load on rescue running insufficiently understood [3-5,16]. Third, most analyses rely primarily on discrete variables, such as peak moments or peak ground reaction forces, even though joint angles, joint moments, ground reaction forces, and

center-of-gravity trajectories change continuously across the stance phase. One-dimensional statistical parametric mapping can evaluate entire biomechanical waveforms and identify the stance-phase regions where task effects occur, complementing discrete linear mixed-effects modelling [17,18]. A combined discrete and time-series approach may therefore provide a more complete understanding of how firefighters adapt their movement control under occupationally realistic constraints.

Accordingly, the present study aimed to determine how fatigue and shoulder-carried load jointly influence movement control during firefighter rescue running, and how these adaptations are reflected in lower-limb mechanical loading and dynamic stability. Specifically, we examined spatiotemporal regulation, lower-limb joint range of motion, joint moments, ground reaction forces, and center-of-gravity motion across pre-fatigue and post-fatigue states under multiple shoulder-carried load conditions. We hypothesized that increasing load and fatigue would not produce uniform changes across all variables, but would instead elicit a coordinated adaptation strategy characterized by altered gait regulation, joint-specific redistribution of mechanical demand, modified ground reaction force patterns, and direction-specific changes in center-of-gravity control. We further expected these adaptations to be most evident during the stance phase, when the lower limb must simultaneously support body-load mass, generate propulsion, and maintain dynamic stability.

Materials and methods

Participants

Seventeen healthy male firefighters were recruited from the Guilin Fire Rescue Detachment, China. Their mean age, height, and body mass were 24.9 ± 3.1 years, 172.8 ± 6.5 cm, and 71.1 ± 7.5 kg, respectively, and their mean duration of firefighting service was approximately 2.3 years. The inclusion criteria were: (1) being an active-duty male firefighter and (2) being in good health. The exclusion criteria were: (1) a history of lower-limb musculoskeletal injury or neurological disorders within the preceding year and (2) the use of medications that could affect motor performance during the testing period.An a priori power analysis was performed using G*Power software (version 3.1.9.7; Heinrich Heine University Düsseldorf, Düsseldorf, Germany) to estimate the minimum required sample size for a repeated-measures ANOVA with within-subject factors. Based on an effect size derived from the η^2 value of 0.26 reported for the maximum knee flexion moment in a previous study (Zhang et al. [5]), with a significance level of 0.05 and statistical power of 0.95, the estimated minimum sample size was six participants. The final sample comprised 17 firefighters.The study protocol was approved by the Human Ethics Committee of Guangxi Normal University (approval number: 20230419001), and all participants provided written informed consent before participation. All methods were performed in accordance with the relevant guidelines and regulations and with the Declaration of Helsinki. Written informed consent was also obtained from all participants for the publication of potentially identifiable images in an online open-access publication.

Experimental design

A repeated-measures experimental design was employed to quantify the independent and combined effects of fatigue state and shoulder-carried load on lower-limb biomechanics and dynamic stability during firefighter rescue running. Fatigue state consisted of two levels (pre-fatigue and post-fatigue), whereas shoulder-carried load consisted of three levels (10, 20, and 30 kg), representing the approximate masses of commonly used firefighting and rescue equipment, including a fire hose, compressed gas cylinder, and fire ladder. All loads were carried on the shoulder ipsilateral to the dominant lower limb to replicate common rescue practice. Each participant completed all six experimental conditions, with three successful trials collected under each condition.

Pre-fatigue and post-fatigue tests were conducted on two separate days with an interval of at least 48 h to minimize residual fatigue. According to the experimental protocol, all participants completed the pre-fatigue session before the post-fatigue session. Within each testing session, load conditions were performed sequentially from 10 to 30 kg. Consequently, neither fatigue state nor load order was randomized, and the potential influence of order effects should be considered when interpreting the findings.

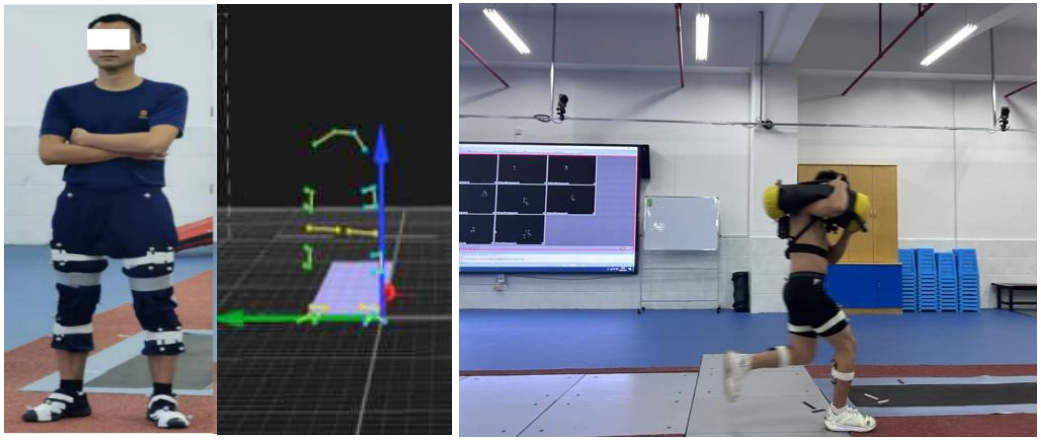

Figure 1. Experimental setup for the firefighter rescue-running task

Instrumentation

Three-dimensional kinematic data were collected using an eight-camera motion capture system (OQUS600+, Qualisys AB, Gothenburg, Sweden) at a sampling frequency of 200 Hz. Ground reaction force data were simultaneously recorded at 1000 Hz using an AMTI force platform (AMTI, Watertown, MA, USA). The motion capture system and force platform were synchronized via an analog-to-digital converter.

Retro-reflective markers (14 mm diameter) were attached to anatomical landmarks and tracking clusters according to the Qualisys lower-limb marker protocol. Raw marker trajectories were labelled, gap-filled when necessary, and preprocessed in Qualisys Track Manager (QTM, Qualisys AB, Gothenburg, Sweden). Kinematic and kinetic variables were subsequently calculated in Visual3D (C-Motion, Germantown, MD, USA). Fatigue induction was performed using a motorized treadmill (MERACH X1PW, China), and heart rate was continuously monitored using a Polar H9 chest-strap heart-rate monitor (Polar Electro, Kempele, Finland).



Figure 2. Experimental setup and instrumentation

Experimental procedures

All testing was conducted in the Sports Biomechanics Laboratory of Guangxi Normal University. Before testing, participants' demographic information, including age, height, body mass, injury history, and firefighting service duration, was recorded. Participants were instructed to avoid strenuous exercise, alcohol consumption, and sleep deprivation during the 24 h preceding each testing session.

At the beginning of each session, participants received standardized instructions regarding the experimental procedures and safety requirements before completing a 10–15 min standardized warm-up consisting of light jogging and dynamic stretching. After a 3–5 min recovery period, reflective markers were attached and a static calibration trial was recorded.

Participants then performed familiarization trials along a 12-m runway to establish an individualized starting position that enabled natural contact of the dominant foot with the force platform. Formal data collection commenced only after at least two successful familiarization trials had been completed. For each rescue-running trial, participants were instructed to accelerate from their individualized starting position and run through the end of the 12-m runway at maximal effort while maintaining the prescribed shoulder-carried load. They were instructed not to slow down or alter their stride to target the force platform.

During the pre-fatigue session, participants completed rescue-running trials while carrying shoulder loads of 10, 20, and 30 kg. Adequate recovery was provided between load conditions to allow heart rate to return close to resting level. During the post-fatigue session, participants repeated the identical protocol immediately following fatigue induction. Rest intervals between trials were minimized to preserve the fatigued state while ensuring participant safety.

A trial was considered successful when the required shoulder-carried posture was maintained throughout the trial, the dominant foot contacted the force platform naturally and completely, and no marker trajectories were lost. Trials failing to satisfy these criteria were discarded and repeated until three successful trials were obtained for each experimental condition.

Fatigue protocol

Fatigue was induced using a graded treadmill-running protocol adapted from previously published protocols. Participants began running at 5 km/h with a 0% incline. The treadmill gradient was increased by 2% every 2 min until reaching 14%, after which the incline remained constant while running speed was increased by 0.5 km/h every minute until volitional exhaustion [16].

Heart rate was continuously monitored using a Polar H9 heart-rate monitor, and perceived exertion was assessed using the Borg 6–20 Rating of Perceived Exertion (RPE) scale [19]. Participants were considered to have reached the fatigued state when all of the following criteria were simultaneously satisfied: (1) RPE $\geq$ 17; (2) heart rate $\geq$ 85% of the age-predicted maximum heart rate (220 − age); and (3) inability to maintain the required treadmill speed despite verbal encouragement. Heart rate and perceived exertion were recorded throughout the fatigue protocol by two investigators to ensure consistency of fatigue assessment.

Data processing and outcome variables

Biomechanical analyses focused on the stance phase of the dominant limb, as this phase is primarily responsible for impact attenuation, body support, propulsion, and dynamic balance during running. Stance was defined from initial contact to toe-off using the vertical ground reaction force. Initial contact and toe-off were identified when the vertical ground reaction force exceeded and fell below 10 N, respectively.

All stance-phase waveforms were time-normalized to 100% of the stance phase before statistical analysis. To maintain consistency with the processed dataset used for SPM analysis, each waveform was resampled to 45 normalized data points.

A three-dimensional lower-limb model was constructed in Visual3D. Hip motion was calculated relative to the pelvis, knee motion relative to the thigh, and ankle motion relative to the shank. Marker trajectories were filtered using a fourth-order zero-lag Butterworth low-pass filter with a cut-off frequency of 14 Hz, whereas ground reaction force data were filtered using a fourth-order zero-lag Butterworth low-pass filter with a cut-off frequency of 50 Hz. Joint moments were calculated using inverse dynamics and normalized to body mass.

Discrete outcome variables included spatiotemporal, kinematic, kinetic, ground reaction force, and center-of-gravity variables. Spatiotemporal variables comprised step length, step width, and stance time. Kinematic variables included hip, knee, and ankle range of motion (ROM), calculated as the difference between the maximum and minimum joint angle during stance. Kinetic variables included peak hip, knee, and ankle joint moments. The discrete ground reaction force outcome reported in Tables 7 and 8 was the maximum vertical component (R_GRF Z) of each exported waveform. Source force values were normalized to participant mass plus carried load (N/kg); for reporting, they were divided by 9.81 m/s² to express force in multiples of the combined body-and-load weight (BW). The anterior–posterior and mediolateral components were evaluated as continuous waveforms using SPM1D. Center-of-gravity displacement was quantified in the mediolateral, anterior–posterior, and vertical directions according to the laboratory coordinate system.

Statistical analysis

Discrete biomechanical variables were analysed using linear mixed-effects models (LMMs) to account for the repeated-measures design and within-participant correlations. To avoid treating repeated technical trials as independent biological observations, the three successful trials were averaged for each participant under each experimental condition before statistical analysis.

For each outcome variable, fatigue state (pre-fatigue and post-fatigue), shoulder-carried load (10, 20, and 30 kg), and their interaction were specified as fixed effects, whereas participant identity was included as a random intercept. The model was specified as:

$$\text{Outcome} \sim \text{Fatigue} \times \text{Load} + (1 \mid \text{Participant})$$

Pre-fatigue and the 10 kg load condition were treated as the reference levels. Type III tests with Satterthwaite approximation were used to evaluate the main effects of fatigue state, load, and their interaction. When significant main effects or interactions were identified, estimated marginal means (EMMs) with Holm-adjusted pairwise comparisons were performed for post hoc analyses. Model assumptions were evaluated by visual inspection of residual-versus-fitted plots and normal Q–Q plots.

Time-continuous biomechanical waveforms were analysed using two-way repeated-measures statistical parametric mapping (SPM1d). Separate SPM analyses were conducted for joint-angle, joint-moment, ground-reaction-force, and centre-of-gravity waveforms. The main effects of fatigue state, shoulder-carried load, and their interaction were evaluated across the entire normalized stance phase. Statistical significance was set at $P < 0.05$. Significant supra-threshold clusters were reported as percentages of the stance phase. When significant interactions were detected, post hoc SPM simple-effects analyses were performed to identify load-specific fatigue effects or fatigue-specific load effects.

Continuous variables are presented as mean ± standard deviation (SD). Statistical analyses were performed using R (version 4.5.0; R Foundation for Statistical Computing, Vienna, Austria) with the lme4, lmerTest, and emmeans packages for LMM analyses, and Python (version 3.14) with the spm1d package for waveform analyses.

3 Results

3.1 Spatiotemporal gait parameters

Table 1. Fixed effects for spatiotemporal gait parameters.

Variable	Fatigue		Load		Fatigue x Load	
	F	P	F	P	F	P
Step length (m)	1.008	0.322	66.006	< 0.001	0.493	0.613
Step width (m)	6.063	0.018	8.454	< 0.001	0.853	0.430
Gait cycle (s)	26.736	< 0.001	0.304	0.739	0.581	0.561

Table 2. Spatiotemporal gait parameters across fatigue and shoulder-carried load conditions.

Variable	fatigue		Load		
	Pre	Post	10kg	20kg	30kg
Step length (m)	1.414 ±0.207	1.471±0.202	1.5474±0.223	1.441a±0.180	1.341ab±0.166
Step width (m)	0.11±0.052	0.080#±0.047	0.100±0.008	0.110±0.007	0.076ab±0.008
Gait cycle (s)	4.568±0.729	6.356#±0.899	5.416±0.167	5.484±0.187	5.486±0.194

Note. Within each outcome, a significant post hoc difference between the pre- and post-fatigue conditions is indicated by "#" following the mean value; "#" denotes a significant difference from the pre-fatigue condition ($P < 0.05$). Significant post hoc differences between load conditions are indicated by "a" and "b" following the mean value; "a" denotes a significant difference from the low-load condition, and "b" denotes a significant difference from the moderate-load condition ($P < 0.05$).

Step length showed a significant main effect of load ($F = 66.006$, $P < 0.001$), but no significant effect of fatigue ($F = 1.008$, $P = 0.322$) or fatigue × load interaction ($F = 0.493$, $P = 0.613$). Mean step length decreased from 1.547 m at 10 kg to 1.441 m at 20 kg and 1.341 m at 30 kg. The post hoc annotations indicate significant differences between 20 and 10 kg, and between 30 kg and both lighter loads ($P < 0.05$).Step width showed significant main effects of fatigue ($F = 6.063$, $P = 0.018$) and load ($F = 8.454$, $P < 0.001$), with no significant interaction ($F = 0.853$, $P = 0.430$). Mean step width decreased from 0.110 m before fatigue to 0.080 m after fatigue ($P < 0.05$). It was also lower at 30 kg (0.076 m) than at 10 kg (0.100 m) and 20 kg (0.110 m), according to the post hoc annotations ($P < 0.05$).Gait cycle duration showed a significant main effect of fatigue ($F = 26.736$, $P < 0.001$), increasing from 4.568 s before fatigue to 6.356 s after fatigue. Neither the load effect ($F = 0.304$, $P = 0.739$) nor the fatigue × load interaction ($F = 0.581$, $P = 0.561$) was significant.

3.2 Joint Range of Motion

Table 3. Joint range of motion across fatigue and shoulder-carried load conditions (n=17)

	State	10 kg	20 kg	30 kg
Hip ROM(°)	Pre	70.13 ± 7.55	70.79 ± 6.34	70.01 ± 7.85
	Post	72.33 ± 7.52	74.14 ± 7.29	74.05 ± 6.20
Knee ROM(°)	Pre	39.48 ± 5.35	37.11 ± 5.74	35.66 ± 7.73
	Post	40.56 ± 5.16	40.07# ± 4.42	39.93# ± 6.64
Ankle ROM(°)	Pre	50.98 ± 4.38	50.32 ± 4.36	51.29 ± 4.81
	Post	52.09 ± 5.70	53.37# ± 6.04	52.61 ± 6.22

Note. Values are observed mean ± SD in degrees; # marks Post versus Pre at the same load when the Holm-adjusted model-based pairwise P < 0.05. The joint load effects were not significant; fixed-effect tests are in Table 4.

Table 4. Fixed effects for joint range of motion from linear mixed-effects models.

	Fatigue			Load			Fatigue × Load		
	F	df	P	F	df	P	F	df	P
Hip ROM(°)	9.71	1, 80	0.003*	0.50	2, 80	0.610	0.27	2, 80	0.762
Knee ROM(°)	13.77	1, 80	<0.001*	3.02	2, 80	0.054	1.54	2, 80	0.220
Ankle ROM(°)	11.43	1, 80	0.001*	0.22	2, 80	0.806	1.30	2, 80	0.278

Note. F(1,80) for fatigue and F(2,80) for load and interaction. * indicates Benjamini–Hochberg-adjusted q < 0.05 across the three primary joint outcomes within the effect family. P values shown are unadjusted.

Fatigue had a main effect on range of motion (ROM) at the hip ($F(1, 80) = 9.71$, unadjusted $P = 0.003$, $q = 0.005$), knee ($F(1, 80) = 13.77$, $P < 0.001$, $q = 0.002$), and ankle ($F(1, 80) = 11.43$, $P = 0.001$, $q = 0.003$). All three effects remained significant after correction across the six primary joint outcomes. Neither load nor the fatigue × load interaction was significant for any ROM outcome (Table 4). The knee load effect was $F(2, 80) = 3.02$ (unadjusted $P = 0.054$, $q = 0.109$).

Across loads, the model-estimated post-minus-pre difference was 3.20° (95% CI 1.15–5.24°) for hip ROM, 2.77° (1.29–4.26°) for knee ROM, and 1.82° (0.75–2.90°) for ankle ROM. Holm-adjusted comparisons at individual loads showed greater post-fatigue knee ROM at 20 kg (difference 2.96°, adjusted $P = 0.049$) and 30 kg (4.28°, $P = 0.004$), and greater ankle ROM at 20 kg (3.05°, $P = 0.005$), as marked in Table 3. No within-load hip ROM comparison remained significant after Holm adjustment.

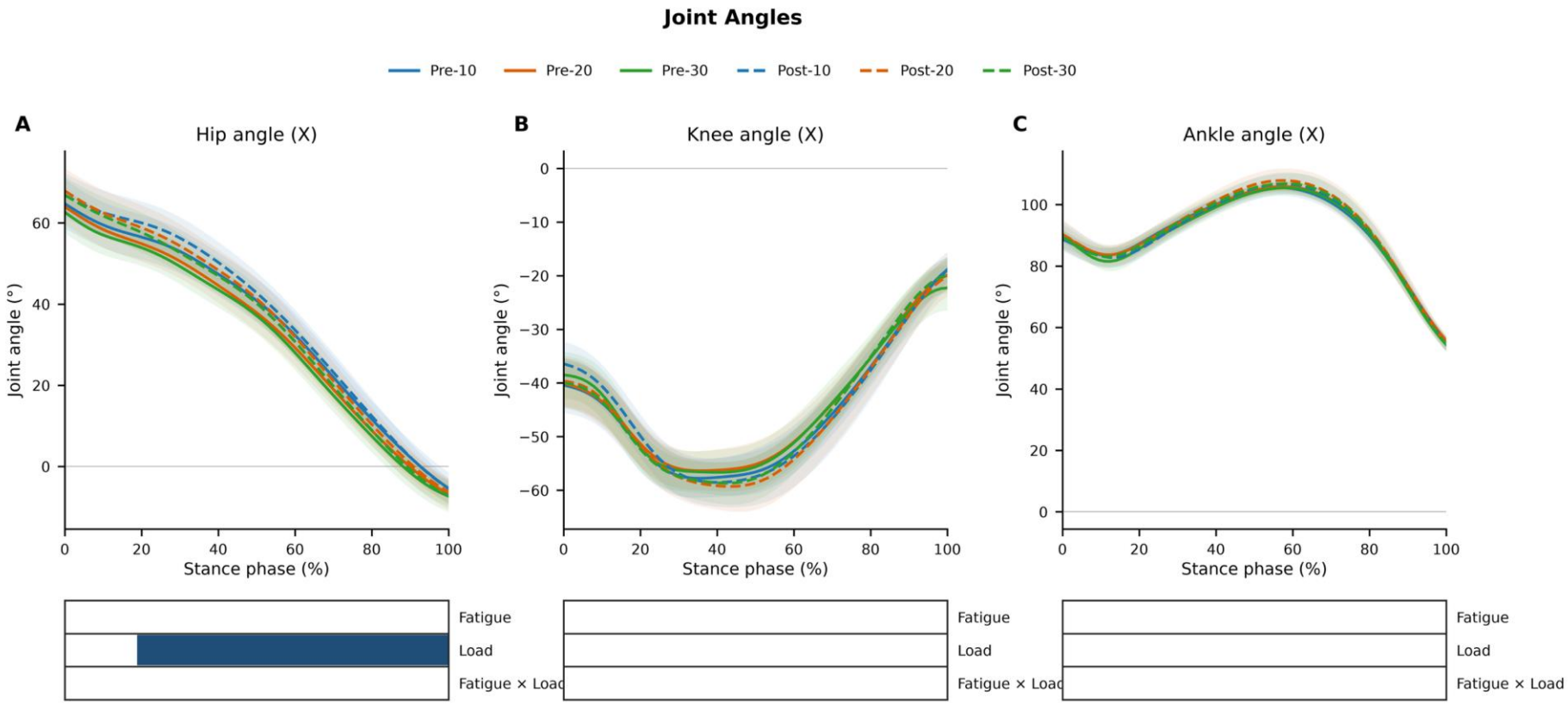

Figure 3. Estimated marginal means of peak hip, knee, and ankle joint moments before and after fatigue across shoulder-carried loads

SPM analysis showed a significant main effect of load on hip joint angle during the stance phase, whereas no significant fatigue main effect or fatigue × load interaction was observed. Specifically, load-related differences in hip angle were detected from approximately 19–100% of stance. No significant SPM clusters were found for knee angle or ankle angle.This indicates that shoulder-carried load mainly affected hip joint angular strategy across most of the stance phase, especially from loading acceptance through mid-stance and push-off. The absence of significant knee and ankle angle clusters suggests that angular adaptations to load were expressed predominantly at the hip rather than through coordinated changes across all lower-limb joints.

3.3 Joint Moments

Table 5. Positive peak joint moments across fatigue and shoulder-carried load conditions (n=17) .

Moment	State	10 kg	20 kg	30 kg
hip moment（N·m/kg）	Pre	0.75 ± 0.40	0.84 ± 0.39	0.97a ± 0.43
	Post	0.82 ± 0.47	1.01a ± 0.43	0.97 ± 0.29
knee moment（N·m/kg）	Pre	2.56 ± 0.62	2.38a ± 0.57	2.21ab ± 0.52
	Post	2.73 ± 0.45	2.44a ± 0.44	2.26ab ± 0.47
ankle moment（N·m/kg）	Pre	0.16 ± 0.13	0.18 ± 0.12	0.18 ± 0.11
	Post	0.22 ± 0.16	0.21 ± 0.14	0.19 ± 0.13

Note. Values are observed mean ± SD; Positive peak is the signed maximum of the moment in the body-mass-normalized export scale. # marks Post versus Pre at the same load; a marks 20 or 30 versus 10 kg within the same state; b marks 30 versus 20 kg within the same state. Markers indicate Holm-adjusted model-based pairwise P < 0.05.

Table 6. Fixed effects for positive peak joint moments from linear mixed-effects models.

Moment	Fatigue			Load			Fatigue × Load		
	F	df	P	F	df	P	F	df	P
hip moment（N·m/kg）	3.23	1, 80	0.076	6.35	2, 80	0.003*	1.15	2, 80	0.322
knee moment（N·m/kg）	4.38	1, 80	0.039	28.87	2, 80	<0.001*	0.84	2, 80	0.435
ankle moment（N·m/kg）	2.19	1, 80	0.143	0.11	2, 80	0.895	0.49	2, 80	0.614

Note. Values are F statistics from linear mixed-effects models. Degrees of freedom were (1, 80) for fatigue and (2, 80) for load and the fatigue × load interaction. For each effect separately, P values for the hip, knee, and ankle outcomes were adjusted using the Benjamini–Hochberg procedure. Reported P values are unadjusted; * denotes an adjusted q value < 0.05. The unstarred knee fatigue effect (unadjusted P = 0.039) did not remain significant after adjustment.

Positive peak hip and knee joint moments showed significant main effects of shoulder-carried load (hip: $F(2, 80) = 6.35$, $P = 0.003$; knee: $F(2, 80) = 28.87$, $P < 0.001$; Table 6). Before fatigue, the hip moment was higher at 30 kg than at 10 kg. After fatigue, it was higher at 20 kg than at 10 kg, as indicated by the Holm-adjusted pairwise comparisons in Table 5. Knee moments were lower at 20 kg than at 10 kg and lower at 30 kg than at both lighter loads in each fatigue state. No significant load effect was observed for the ankle moment ($F(2, 80) = 0.11$, $P = 0.895$).No fatigue × load interaction was significant for the hip, knee, or ankle moment (all $P \geq 0.322$). The fatigue main effects for the hip ($P = 0.076$) and ankle ($P = 0.143$) were not significant. Although the knee fatigue effect had an unadjusted P value of 0.039, it did not remain significant after the specified Benjamini–Hochberg correction. Thus, the discrete peak-moment results primarily support load-related changes in hip and knee moments, without evidence that the effect of fatigue differed by load.

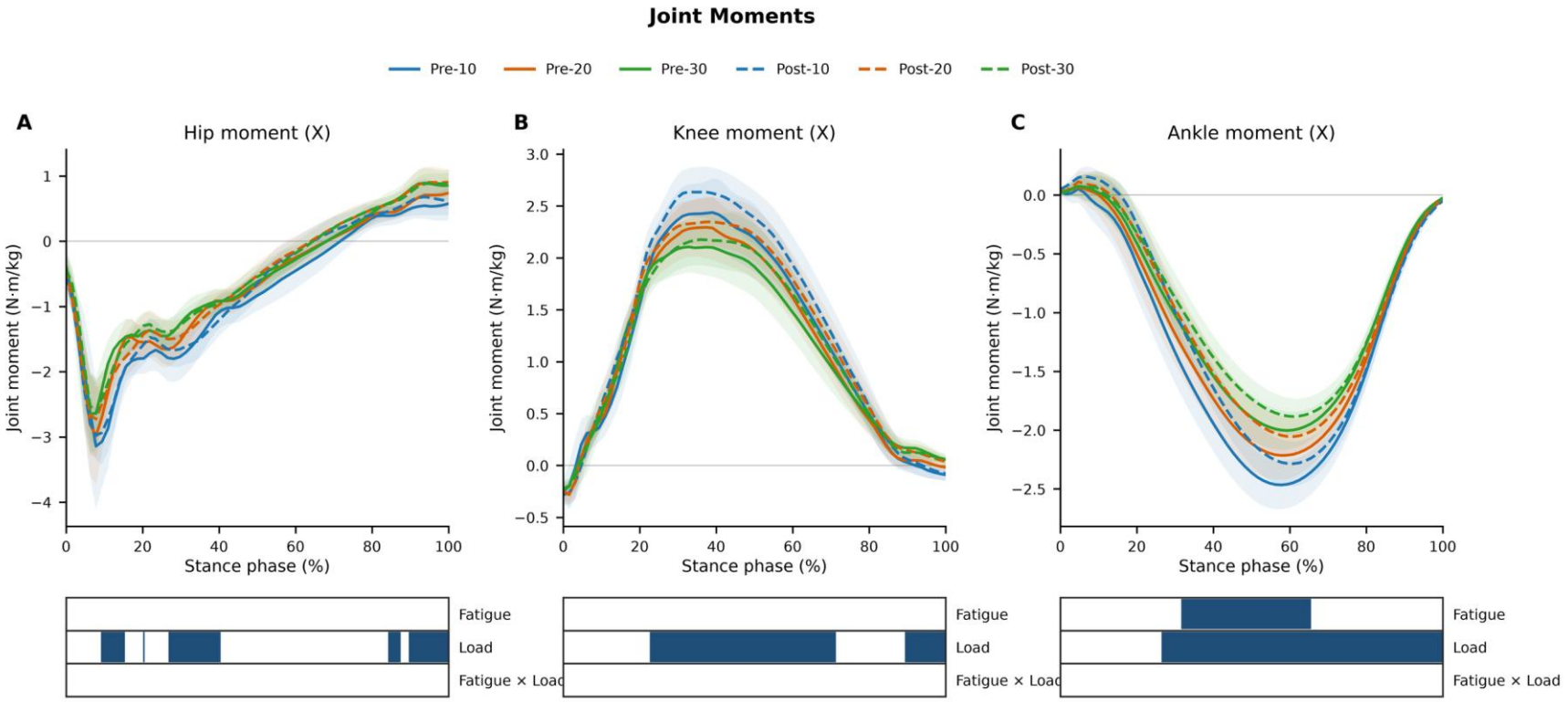

Figure 4. SPM analysis of lower-limb joint moment waveforms during firefighter rescue running.

SPM analysis revealed marked load effects on lower-limb joint moments. For hip moment, significant load effects occurred during 9–15%、20–21%、27–40%、84–87% and 90–100% of stance. For knee moment, significant load effects were observed during 23–71% and 89–100% of stance. For ankle moment, a significant fatigue main effect appeared during 32–66% of stance, while load effects were observed during 26–100% of stance. No clear fatigue × load interaction clusters were detected for joint moments.

These findings suggest that external load strongly altered the mechanical demand of the hip, knee, and ankle during stance. Hip moment differences appeared in early stance and terminal stance, indicating altered impact absorption and push-off control. Knee moment was load-sensitive across a broad mid-stance interval, suggesting that the knee played an important role in supporting and transferring load. Ankle moment showed both fatigue and load effects, indicating that fatigue may particularly influence ankle mechanical output during mid-stance.

3.4 Ground Reaction Forces

Table 7. Peak vertical ground reaction force (multiples of combined body-and-load weight, BW) across fatigue and shoulder-carried load conditions (n = 17).

	Load	Pre-fatigue	Post-fatigue
Peak vertical GRF (BW)	10 kg	2.41 ± 0.45	2.24 ± 0.26
	20 kg	2.17a ± 0.40	2.01a ± 0.25
	30 kg	1.99ab ± 0.29	1.86a ± 0.21

Note. Values are observed mean ± SD in BW. # denotes Post versus Pre at the same load; a denotes 20 or 30 versus 10 kg within the same fatigue state; b denotes 30 versus 20 kg within the same fatigue state. Markers indicate Holm-adjusted model-based $P < 0.05$.

Table 8. Fixed effects from linear mixed-effects models for peak vertical ground reaction force (BW).

	Effect	df	F	P
Peak vertical GRF (BW)	Fatigue	1, 80	11.41	0.001*
	Load	2, 80	25.72	<0.001*
	Fatigue x Load	2, 80	0.07	0.935

Note. Models included fatigue, load, and their interaction as fixed effects, with analysis sample as a random intercept. df = numerator and denominator degrees of freedom. As in Section 3.2, * indicates Benjamini–Hochberg-adjusted $q < 0.05$ within each effect family; the Section 3.4 family contains one prespecified GRF outcome, so q equals the unadjusted P. P values shown are unadjusted. Pairwise markers in Table 7 use Holm adjustment.

Peak vertical ground reaction force (GRF) showed main effects of fatigue ($F(1, 80) = 11.41$, unadjusted $P = 0.001$, $q = 0.001$) and load ($F(2, 80) = 25.72$, $P < 0.001$, $q < 0.001$), with no fatigue × load interaction ($F(2, 80) = 0.07$, $P = 0.935$; Table 8). The observed means were lower after fatigue at all three loads and decreased as load rose from 10 to 30 kg in both fatigue states (Table 7). None of the three within-load pre- versus post-fatigue comparisons remained significant after Holm adjustment.

Within the pre-fatigue state, peak GRF was lower at 20 than 10 kg (Holm-adjusted $P = 0.006$), at 30 than 20 kg ($P = 0.028$), and at 30 than 10 kg ($P < 0.001$). After fatigue, peak GRF was lower at 20 and 30 kg than at 10 kg ($P = 0.009$ and $P < 0.001$, respectively); the 30 versus 20 kg comparison was not significant ($P = 0.065$).

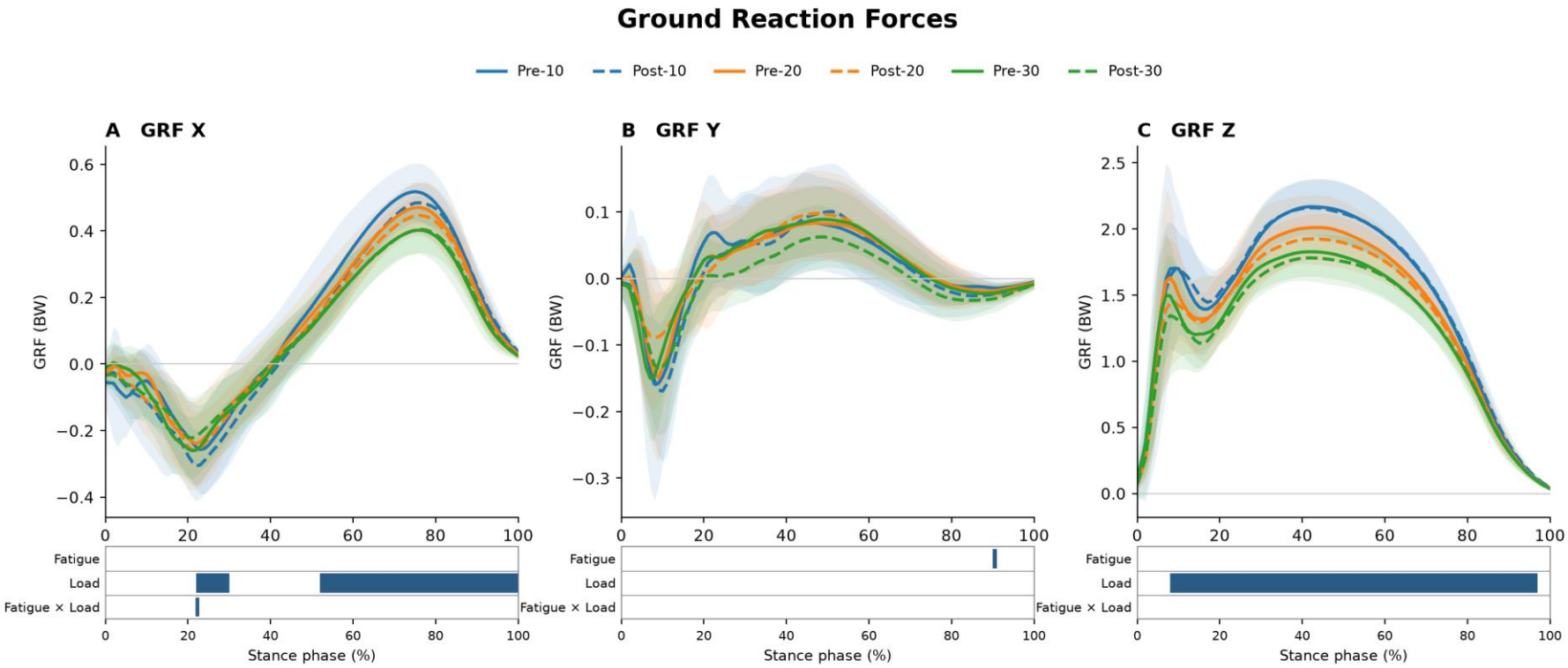

Figure 5. Ground reaction force components across the stance phase before and after fatigue at each shoulder-carried load. All force components are expressed relative to combined body-and-load weight (BW). Lines show condition means, shading shows ±1 SD, and blue bars mark significant SPM1D clusters (fieldwise $P < 0.05$).

SPM analysis showed significant load effects on GRF X during 22–30% and 52–100% of stance, and on GRF Z during 8–97% of stance. GRF Y showed a very narrow fatigue-related significant interval at approximately 90–91% of stance. A very short interaction-related cluster was observed for GRF X around 22% of stance, but because this interval was extremely brief, it should be interpreted cautiously.

These results indicate that shoulder-carried load substantially influenced ground reaction force patterns, especially in the mediolateral/anterior-posterior and vertical components. The broad GRF Z load effect suggests that vertical loading was affected across nearly the entire stance phase, from early weight acceptance to push-off. GRF X load effects during early and late stance may reflect altered lateral or braking-propulsive control under heavier carried loads.

3.5 Center-of-Gravity Displacement

Table 9. Observed mean and standard deviation of anteroposterior, mediolateral, and vertical COG excursion across fatigue and shoulder-carried load conditions (n = 17).

	Load	Pre-fatigue	Post-fatigue
Anteroposterior COG（m）	10 kg	0.955 ± 0.093	1.002# ± 0.104
	20 kg	0.963 ± 0.093	1.020# ± 0.110
	30 kg	0.988 ± 0.078	1.007 ± 0.114
Mediolateral COG（m）	10 kg	0.027 ± 0.022	0.028 ± 0.019
	20 kg	0.027 ± 0.019	0.036 ± 0.022
	30 kg	0.033 ± 0.026	0.027 ± 0.016
Vertical COG（m）	10 kg	0.069 ± 0.014	0.072 ± 0.014
	20 kg	0.063 ± 0.014	0.065a ± 0.012
	30 kg	0.060a ± 0.010	0.063a ± 0.010

Note. Values are observed mean ± SD of maximum-minus-minimum COG position (m) in the specified laboratory axis; # marks Post versus Pre at the same load; a marks 20 or 30 versus 10 kg within the same state; b marks 30 versus 20 kg within the same state. Markers indicate Holm-adjusted model-based pairwise $P < 0.05$. Axis directions require confirmation against the laboratory coordinate convention.

Table 10. Fixed effects from linear mixed-effects models for COG excursion.

	Effect	df	F	P
Anteroposterior COG（m）	Fatigue	1, 80	24.74	<0.001*
	Load	2, 80	1.76	0.179
	Fatigue x Load	2, 80	1.92	0.153
Mediolateral COG（m）	Fatigue	1, 80	0.17	0.684
	Load	2, 80	0.47	0.628
	Fatigue x Load	2, 80	1.48	0.234
Vertical COG（m）	Fatigue	1, 80	2.26	0.136
	Load	2, 80	9.98	<0.001*
	Fatigue x Load	2, 80	0.12	0.886

Note. Models included fatigue, load, and their interaction as fixed effects, with analysis sample as a random intercept. df = numerator and denominator degrees of freedom. As in Section 3.2, * indicates Benjamini–Hochberg-adjusted $q < 0.05$ across the three prespecified COG-axis outcomes within each effect family. P values shown are unadjusted. Pairwise markers in Table 9 use Holm adjustment. Axis directions require confirmation against the laboratory coordinate convention.

Anteroposterior COG excursion showed a fatigue main effect ($F(1, 80) = 24.74$, unadjusted $P < 0.001$, $q < 0.001$), without a load effect ($P = 0.179$) or fatigue × load interaction ($P = 0.153$; Table 10). Post-fatigue anteroposterior excursion was greater at 10 kg (mean difference 0.047 m; Holm-adjusted $P = 0.003$) and 20 kg (0.058 m; $P < 0.001$), but not at 30 kg ($P = 0.188$; Table 9). No fixed effect was detected for mediolateral excursion (all unadjusted $P \geq 0.234$).

Vertical COG excursion showed a load main effect ($F(2, 80) = 9.98$, unadjusted $P < 0.001$, $q < 0.001$), without a fatigue effect ($P = 0.136$) or interaction ($P = 0.886$). It was lower at 30 versus 10 kg before fatigue (Holm-adjusted $P = 0.005$) and at 20 and 30 versus 10 kg after fatigue ($P = 0.037$ and $P = 0.017$, respectively; Table 9).

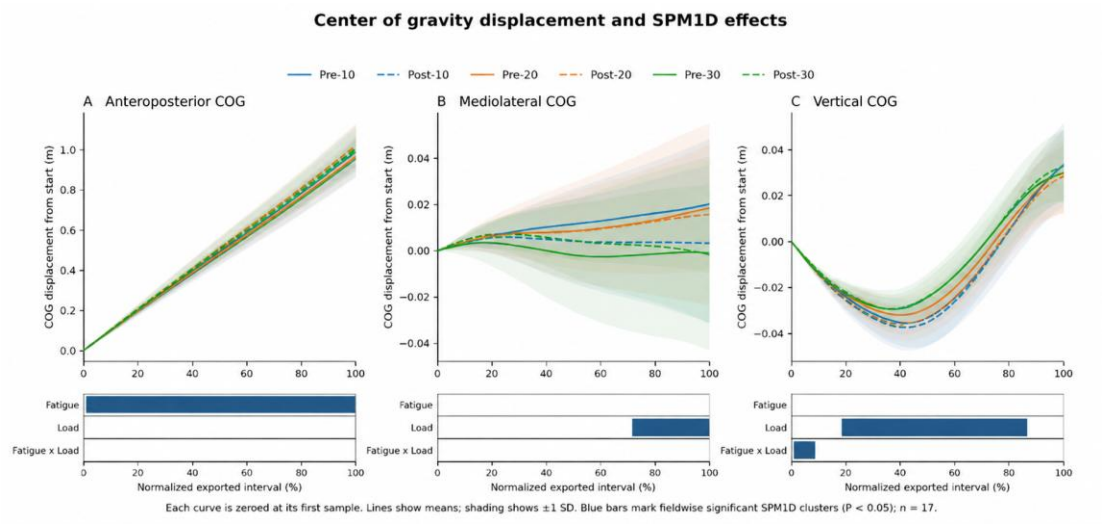

Figure 6. Center-of-gravity (COG) displacement trajectories and SPM1D results across fatigue states and shoulder-carried loads. Panels A–C show COG displacement in the anteroposterior, mediolateral, and vertical directions, respectively. Each trajectory was referenced to its first sample. Solid lines represent pre-fatigue conditions, dashed lines represent post-fatigue conditions, and colors indicate 10 kg (blue), 20 kg (orange), and 30 kg (green) loads. Shaded areas indicate ±1 standard deviation. Blue bars beneath each panel indicate stance intervals with significant main effects of fatigue or load, or a fatigue × load interaction, identified by SPM1D (fieldwise $P < 0.05$). The horizontal axis represents the normalized exported interval; n = 17.

For first-sample-referenced COG displacement, SPM1D found a fatigue effect on the anteroposterior trajectory from 1% to 100% of the normalized exported interval (cluster $P < 0.001$), a load effect on the mediolateral trajectory from 71.6% to 100% ($P = 0.002$), and a load effect on the vertical trajectory from 18.4% to 86.6% ($P < 0.001$; Figure 6). A short fatigue × load cluster occurred in the vertical trajectory from 1.0% to 8.7% ($P = 0.036$). No anteroposterior fatigue × load cluster remained after first-sample referencing.Figure 6 reports omnibus SPM1D effects on directional trajectories, whereas Tables 9–10 report maximum-minus-minimum excursions. A significant waveform cluster need not imply a significant excursion effect, and an omnibus cluster does not identify a specific load pair. The anteroposterior fatigue effect is supported by both waveform and excursion analyses, but these measures do not quantify dynamic stability.

Discussion

The findings were outcome-specific rather than a uniform increase in mechanical demand. Greater load was associated with shorter steps, divergent positive peak hip and knee moments, lower peak vertical GRF, and altered vertical COG excursion. Fatigue increased ROM at all three joints and anteroposterior COG excursion; step width

also decreased in the reported gait analysis. Most fatigue × load tests were not significant. The data therefore support distinct load- and fatigue-related adaptations, but do not establish a synergistic interaction, a protective response, or loss of dynamic stability.

Gait regulation and joint motion

Step length decreased as the shoulder-carried load increased, while step width varied with both fatigue and load. Similar task-level gait changes have been reported in firefighters carrying asymmetric hose loads and in rescue-running studies with different carried objects [3,5]. Mao et al. also found load-sensitive sprint speed, step length, and stance time in firefighters [16]. These comparisons support the task relevance of the present gait findings, although differences in carriage method, protective equipment, running distance, and speed prevent direct numerical comparison.

The joint-angle findings clarify why the discrete and waveform analyses should be read together. Load did not significantly change hip, knee, or ankle ROM, yet the hip-angle waveform differed over much of the normalized interval. ROM is the distance between a trial's maximum and minimum angle; two curves can differ in offset, timing, or local shape while retaining similar ROM. In contrast, fatigue increased ROM at all three joints, but only selected knee and ankle within-load comparisons survived Holm adjustment. Thus, the evidence supports fatigue-related increases in joint excursion but no monotonic load effect on knee ROM.

A shorter step and narrower step width may reflect altered foot-placement choices, but their functional purpose cannot be inferred from these outcomes alone. In controlled-speed vest running, added load increased contact time, leg stiffness, and joint flexion at contact [11]; the present shoulder-carry task differs in load placement and did not provide verified condition-specific running speeds. Accordingly, a cautious gait strategy is a plausible interpretation, not a demonstrated mechanism. Future speed-matched trials and foot-placement measurements could determine whether these adjustments are primarily mechanical consequences of added mass or active regulation of the body–load system.

Joint moments and the limits of mechanical interpretation

The load response was not a simple rise in every joint moment. Positive peak hip moment increased with load, whereas positive peak knee moment decreased; the ankle positive peak did not show a significant fixed effect. The nominal knee fatigue result did not survive the six-outcome correction, and no discrete fatigue × load interaction was present. There was therefore no evidence of a fatigue-specific hip response at 20 kg. The positive-peak results instead indicate that selected net-moment amplitudes changed in opposite directions across joints.

SPM1D adds a temporal layer: load effects on hip and knee moments occurred in several stance regions, while the ankle moment differed over a broad interval despite an unchanged positive maximum. A peak statistic discards the timing and sign of the remainder of the waveform. More importantly, net joint moment is not synonymous with muscle force, joint power, or work. Those quantities require angular velocity, time integration, and, for muscle-specific claims, additional modeling or electromyography. Speed-dependent shifts in muscle contributions have been demonstrated with musculoskeletal simulation [21], and fatigue-related ankle-to-hip work changes have been reported in female recreational runners [20], but the present measurements cannot establish an analogous distal-to-proximal transfer.

The opposite directions of the hip and knee positive peaks could arise from changes in posture, ground-force moment arms, or task speed. Since the axes and sign conventions of the exported moments are central to interpretation, the safest conclusion is that load altered joint-specific net-moment patterns, not that it redistributed a known amount of mechanical work. Quantifying positive and negative joint work and their contributions would test whether the apparent moment changes constitute true energy redistribution.

These findings suggest a practical assessment target rather than a proven intervention: loaded running tests should examine more than a single peak moment or unloaded sprint time. Whether strengthening a particular joint or trunk muscle improves rescue performance or reduces injury remains to be tested in an intervention study.

External force under load and fatigue

Peak vertical GRF decreased as load increased and showed a fatigue main effect, although no individual pre- versus post-fatigue contrast at a given load survived Holm adjustment. A broad vertical GRF waveform load effect supports a change across stance rather than at only one instant. This pattern differs from controlled-speed, weight-vest running, where greater load increased peak vertical GRF [11], and from military load-carriage walking, where greater carried mass increased vertical and anterior–posterior forces [22]. It resembles the lower vertical GRF observed in a firefighter gas-can rescue task performed at a slower self-selected pace [5].

These differences highlight the importance of task and speed. Carriage asymmetry, footwear, rescue object, force normalization, and self-selected speed can all affect measured external force; none was isolated here. Lower peak GRF should therefore be described as an observed external-force change, not evidence that participants deliberately cushioned impact. Moreover, GRF peaks do not reliably track internal tibial load across running speeds and slopes [13]. Without loading rate, impulse, joint contact forces, or tissue-level modeling, the present decrease cannot be translated into lower tissue stress or injury risk.

The brief mediolateral fatigue and anteroposterior interaction SPM clusters are less robust in duration than the broad load effects. Their presence does not overturn the nonsignificant discrete fatigue × load test for peak vertical GRF because the analyses address different force directions and portions of the waveform. Independent replication and corrected pairwise waveform comparisons would be needed before assigning a task-level mechanism to these short intervals.

COG motion is not a direct stability measure

Anteroposterior COG excursion increased after fatigue at 10 and 20 kg, vertical excursion varied with load, and mediolateral excursion had no significant fixed effect. First-sample-referenced waveforms showed a broad anteroposterior fatigue effect, late mediolateral load differences, and a mid-interval vertical load effect, plus a short early vertical interaction. The anteroposterior waveform and excursion results together show greater recorded forward travel over the exported interval after fatigue at selected loads. They do not show whether speed, contact duration, interval boundaries, or movement regulation produced this difference.

COG excursion alone lacks the information required to quantify dynamic stability. Stability measures consider where the center of mass is moving relative to the base of support, often using COG velocity, foot placement, and the extrapolated center of mass or margin of stability [14,23]. Greater forward displacement over an exported interval does not by itself indicate poorer balance; it can change with task speed and the duration or boundaries of the analyzed interval. The current data therefore describe directional body motion but cannot establish a smaller stability margin or a higher probability of falling.

This distinction matters for occupational interpretation. Step width narrowed after fatigue, but mediolateral COG excursion showed no significant fixed effect. A load effect in the later mediolateral waveform does not identify which loads differ or demonstrate compromised lateral control. To test whether shoulder-carried load changes balance, future work should include the carried object in the whole-system COG model and relate COG position and velocity to foot placement, center of pressure, and stability margins.

Integrated interpretation and practical implications

Taken together, the results describe a set of measurable adaptations rather than a proven causal chain. Added load was most consistently reflected in step length, joint net moments, vertical GRF, and vertical COG excursion; fatigue was reflected in joint ROM and anteroposterior COG excursion. The rarity of significant interactions argues against claiming a general combined fatigue-and-load amplification. The data also cannot identify whether the lower GRF caused the moment changes or whether either response preserved stability. An asymmetric load may impose additional trunk and pelvic demands, but trunk moments and muscle activation were not measured here.

For practice, these findings support testing rescue running under representative loads and documenting both discrete peaks and waveform changes. They do not yet justify a specific injury-prevention prescription. Speed-matched experiments, reversed shoulder-carry side, complete three-dimensional net moments, joint power and work, electromyography, and direct balance measures would help distinguish altered task pacing from mechanical compensation and test whether a particular training approach improves performance or reduces adverse outcomes.

Limitations and future directions

Load increased in a fixed order, and the pre-fatigue session always preceded the post-fatigue session; order, learning, and recovery may therefore be confounded with the intended factors. Verified condition-level running speed was unavailable, limiting interpretation of step length, GRF, and forward COG excursion. The precise physical scale of the normalized force export requires confirmation. COG excursion was not referenced to the foot or base of support, and no perturbation, fall, injury, joint-work, or muscle-force outcome was collected. Findings from 17 male analysis samples and this laboratory runway may not generalize to other firefighters, protective equipment, terrain, or prolonged operations. The brief waveform clusters should be replicated before they are given functional significance.

Conclusion

Fatigue and shoulder-carried load produced distinct changes in measured rescue-running mechanics. Greater load was associated with shorter steps, joint-specific positive peak moment responses, lower peak vertical GRF, and altered vertical COG excursion; fatigue increased lower-limb ROM and anteroposterior COG excursion. Most fatigue × load interactions were absent. These findings support an account of task-dependent biomechanical adaptation, while the consequences for dynamic stability, internal tissue loading, and injury risk remain untested.

Conflict of Interest

The authors declare that the research was conducted in the absence of any commercial or financial relationships that could be construed as a potential conflict of interest.

Author Contributions

M.C. contributed to the study conception and design, data collection, data analysis and interpretation, and drafting of the manuscript. J.W. contributed to data collection, data processing, and interpretation of the results. G.F. contributed to the study design, methodology, supervision, and critical revision of the manuscript. W.L. contributed to the study conception, supervision, project administration, and critical revision of the manuscript. All authors reviewed and approved the final version of the manuscript.

Data Availability Statement

The datasets generated and/or analysed during the current study are available from the corresponding author on reasonable request.

References

1. Orr R, Simas V, Canetti E, Schram B. A profile of injuries sustained by firefighters: a critical review. International Journal of Environmental Research and Public Health. 2019;16(20):3931. doi:10.3390/ijerph16203931.
2. Tahernejad S, Farahi-Ashtiani I, Veisani Y, Ghaffari S, Sahebi A, Makki F. A systematic review and meta-analysis of musculoskeletal disorders among firefighters. Journal of Safety Research. 2024;88:374-381. doi:10.1016/j.jsr.2023.11.009.
3. Park K, Sy JF, Horn GP, Kesler RM, Petrucci MN, Rosengren KS, Hsiao-Wecksler ET. Assessing gait changes in firefighters after firefighting activities and while carrying asymmetric loads. Applied Ergonomics. 2018;70:44-50. doi:10.1016/j.apergo.2018.01.016.
4. Park H, Kim S, Morris K, Moukperian M, Moon Y, Stull J. Effect of firefighters' personal protective equipment on gait. Applied Ergonomics. 2015;48:42-48. doi:10.1016/j.apergo.2014.11.001.
5. Zhang X, Feng H, Liu X, Gao P, Guo P, Tang S, Nie X, Feng T, Liu W. Biomechanical characterization of firefighters running under different rescue tasks. Scientific Reports. 2024;14:1813. doi:10.1038/s41598-024-52440-6.
6. Zandbergen MA, Marotta L, Bulthuis R, Buurke JH, Veltink PH, Reenalda J. Effects of level running-induced fatigue on running kinematics: a systematic review and meta-analysis. Gait & Posture. 2023;99:60-75. doi:10.1016/j.gaitpost.2022.09.089.

7. Trowell D, Kenneally-Dabrowski C, Bonacci J. Effects of running-induced fatigue on joint kinematics and kinetics during overground running: a systematic review and meta-analysis. Sports Biomechanics. 2025;24(11):3109-3135. doi:10.1080/14763141.2024.2353390.

8. Choudhary PK, Choudhary S, Saha S, Rajpoot YS, Ciocan VC, Voinea NL, Pavel SI, Sufaru C. Lower-limb biomechanical adaptations to exercise-induced fatigue during running: a systematic review of injury-relevant mechanical changes. Life. 2026;16(2):272. doi:10.3390/life16020272.

9. Möhler F, Ringhof S, Debertin D, Stein T. Influence of fatigue on running coordination: a UCM analysis with a geometric 2D model and a subject-specific anthropometric 3D model. Human Movement Science. 2019;66:133-141. doi:10.1016/j.humov.2019.03.016.

10. Clermont CA, Pohl AJ, Ferber R. Fatigue-related changes in running gait patterns persist in the days following a marathon race. Journal of Sport Rehabilitation. 2020;29(7):934-941. doi:10.1123/jsr.2019-0206.

11. Silder A, Besier T, Delp SL. Running with a load increases leg stiffness. Journal of Biomechanics. 2015;48(6):1003-1008. doi:10.1016/j.jbiomech.2015.01.051.

12. Wang H, Frame J, Ozimek E, Leib D, Dugan EL. Influence of fatigue and load carriage on mechanical loading during walking. Military Medicine. 2012;177(2):152-156. doi:10.7205/MILMED-D-11-00210.

13. Matijevich ES, Branscombe LM, Scott LR, Zelik KE. Ground reaction force metrics are not strongly correlated with tibial bone load when running across speeds and slopes: implications for science, sport and wearable tech. PLoS ONE. 2019;14(1):e0210000. doi:10.1371/journal.pone.0210000.

14. Bruijn SM, Meijer OG, Beek PJ, van Dieen JH. Assessing the stability of human locomotion: a review of current measures. Journal of the Royal Society Interface. 2013;10(83):20120999. doi:10.1098/rsif.2012.0999.

15. Rankin BL, Buffo SK, Dean JC. A neuromechanical strategy for mediolateral foot placement in walking humans. Journal of Neurophysiology. 2014;112(2):374-383. doi:10.1152/jn.00138.2014.

16. Mao C, Wang Z, Zhang X, Ma X, Zeng S, Hao Y, Liu W, Miao Y. Fatigue state and external load effects on firefighter sprinting biomechanics. Frontiers in Bioengineering and Biotechnology. 2025;13:1677575. doi:10.3389/fbioe.2025.1677575.

17. Serrien B, Goossens M, Baeyens JP. Statistical parametric mapping of biomechanical one-dimensional data with Bayesian inference. International Biomechanics. 2019;6(1):9-18. doi:10.1080/23335432.2019.1597643.

18. Yona T, Kamel N, Cohen-Eick G, Ovadia I, Fischer A. One-dimension statistical parametric mapping in lower limb biomechanical analysis: a systematic scoping review. Gait & Posture. 2024;109:133-146. doi:10.1016/j.gaitpost.2024.01.018.

19. Borg GAV. Psychophysical bases of perceived exertion. Medicine & Science in Sports & Exercise. 1982;14(5):377-381. doi:10.1249/00005768-198205000-00012.

20. Quan W, Ren F, Xu D, Gusztav F, Baker JS, Gu Y. Effects of fatigue running on joint mechanics in female runners: a prediction study based on a partial least squares algorithm. Frontiers in Bioengineering and Biotechnology. 2021;9:746761. doi:10.3389/fbioe.2021.746761.

21. Dorn TW, Schache AG, Pandy MG. Muscular strategy shift in human running: dependence of running speed on hip and ankle muscle performance. Journal of Experimental Biology. 2012;215:1944-1956. doi:10.1242/jeb.064527.

22. Birrell SA, Hooper RH, Haslam RA. The effect of military load carriage on ground reaction forces. Gait & Posture. 2007;26(4):611-614. doi:10.1016/j.gaitpost.2006.12.008.

23. Hof AL, Gazendam MGJ, Sinke WE. The condition for dynamic stability. Journal of Biomechanics. 2005;38(1):1-8. doi:10.1016/j.jbiomech.2004.03.025.